Chip-based optical isolator and nonreciprocal parity-time symmetry induced by stimulated Brillouin scattering

Jiyang Ma[1], Jianming Wen[2], Yong Hu[1], Shulin Ding[1], Xiaoshun Jiang[1*], Liang Jiang[3], and Min Xiao[1,4*]

[1]National Laboratory of Solid State Microstructures, College of Engineering and Applied Sciences, and School of Physics, Nanjing University, Nanjing 210093, China

[2]Department of Physics, Kennesaw State University, Marietta, Georgia 30060, USA

[3]Department of Applied Physics and Yale Quantum Institute, Yale University, New Haven, Connecticut 06511, USA.

[4]Department of Physics, University of Arkansas, Fayetteville, Arkansas 72701, USA

Realization of chip-scale nonreciprocal optics such as isolators and circulators is highly demanding for all-optical signal routing and protection with standard photonics foundry process. Owing to the significant challenge for incorporating magneto-optical materials on chip, the exploration of magnetic-free alternatives has become exceedingly imperative in integrated photonics. Here, we demonstrate a chip-based, tunable all-optical isolator at the telecommunication band based upon bulk stimulated Brillouin scattering (SBS) in a high-Q silica microtoroid resonator. This device exhibits remarkable characteristics over most state-of-the-art implements, including high isolation ratio, no insertion loss, and large working power range. Thanks to the guided acoustic wave and accompanying momentum-conservation condition, bulk SBS also enables us to realize the first nonreciprocal parity-time symmetry in two directly-coupled microresonators. The breach of time-reversal symmetry further makes the design a versatile arena for developing many formidable ultra-compact devices such as unidirectional single-mode Brillouin lasers and supersensitive photonic sensors.

L4-39: Lasers and Nonlinear Optics

Integrated photonic circuits demand dynamic optical isolation for advanced signal processing and communications. For the time-reversal symmetry retained in light-matter interaction, unfortunately, light wave transport in any linear, time-invariant optical system complies with the Lorentz reciprocity [1,2]. To violate such reciprocity and obtain asymmetric transmission, it essentially requires to break the time-reversal symmetry. In optics this is typically achievable by employing the magneto-optic Faraday effect. Despite its commercial success, such a well-established approach poses a severe challenge [3,4] for the incorporation with chip-scale photonics due to fabrication complexity with the mature complementary metal-oxide semiconductor (CMOS) technique and difficulty in locally confining magnetic fields as well as significant material losses. As a result, a vibrant search for different physical principles to obtain magnetic-free optical nonreciprocity has garnered a vast impetus in recent years. Alternative methods mostly resort to indirect inter-band transitions [5,6], nonlinear parametric amplification [7,8], thermo-optic effect [9], opto-acoustic interaction [10], Raman amplification [11], stimulated Brillouin scattering (SBS) [12,13], Bragg scattering [14], gain/absorption saturation [15], Kerr nonlinearities [16,17], optomechanical interactions [18-25], and mimicked nonlinear nonadiabatic quantum jumps [26]. Of these schemes, asymmetric optical transmission is mostly experimented with only injecting a light wave in either forward

or backward direction but never both, except the works [7,17,24]. The drawbacks in this type of implementation were questioned in a theoretical study [27], where they showed simultaneous presence of signals from both sides incapable providing complete isolation for Kerr or Kerr-type nonlinearities, due to dynamic reciprocity.

In parallel to the rapid progress on on-chip optical nonreciprocity, there has been an intense research interest in non-Hermitian photonic systems [28,29]. This originates from the observation [30] that certain non-Hermitian Hamiltonians retaining the combined parity-time (PT) symmetry may have real spectra as long as a non-Hermitian parameter reaches above a specific threshold value. At threshold, PT symmetry breaking spontaneously occurs, where the system transitions to a new phase associated with a pair of complex eigenvalues. Regardless of much theoretical success in PT-symmetric quantum theory [31,32], it becomes highly challenging in search of such an elusive Hamiltonian in real physical world. On the other hand, experiments with photonics can be intrinsically non-Hermitian due to the co-existence of gain and loss. Indeed, subsequent works [15,33-44] have undermined their relevance of quantum origin, and readily shown striking PT phase transitions in various optical settings by interleaving balanced gain and loss regions. The associated exceptional spectral properties thereupon translate into unique propagation and scattering behaviors for light, including power oscillations [34], unidirectional invisibility [35], coherent perfect laser absorbers [36], single-mode lasers [37,38] and supersensitive sensors [39,40].

Thanks to the directional momentum conservation in SBS, it enables to construct an on-chip optical isolator with only one Brillouin cavity. Moreover, this directionality can break down the reciprocity in PT symmetry where a Brillouin cavity is coupled with a passive resonator. In other words, in this latter case, the features on observing PT symmetry from two directions will behave differently, and we name this phenomenon nonreciprocal PT symmetry. We notice that Ref. [45] questioned whether it's possible to build an optical isolator through PT symmetry. It turns out that this problem could be addressed by adopting our system. Moreover, nonreciprocal PT symmetry lifts up the degeneracy of the two EPs, which may lead to many important potential applications [46, 47].

Here we experimentally demonstrate, for the first time, a chip-based nonmagnetic optical isolator in high-Q silica microtoroid [48] resonator enabled by *bulk* SBS, in which coherent optically-driven acoustic waves can give rise to highly unidirectional photon-phonon interactions. Although SBS [49,50] is deemed as the strongest of all optical nonlinear processes, exciting SBS in a chip-scale device is technically challenging because of the stringent requirements on materials and device geometry [51]. In contrast to previous cavity-optomechanical schemes [18-25], our platform remarkably exhibits many compelling features including larger isolation ratio, wider bandwidth, and much higher mechanical frequency. Utilizing surface Brillouin excitation, for instance, the isolation bandwidth was achieved only at the 100 KHz level and the mechanical frequencies about 100 MHz. While in our platform, the bandwidth is extended to 0.57 MHz and the mechanical frequency up to 10 GHz. Essential for practical applications, the high frequency feature of the bulk SBS allows the pump light to be easily filtered from the signal field. By harvesting the directional momentum conservation inherent in the SBS process, we further report the first observation of nonreciprocal PT symmetry in two coupled microtoroid cavities with balanced gain and loss, where the bulk SBS is exploited to produce direction-sensitive gain in the Brillouin cavity. Fully

compatible with the current CMOS procedure, besides the application for isolators and circulators, the structure could be configured for a number of demanding chip-based devices including, but not limited to, unidirectional single-mode Brillouin PT lasers and bi-scale ultrasensitive sensors.

Experimental Results.- The physical process of bulk Stimulated Brilluin Scattering [52-54] is described in the first section of supplementary information. This process is schematically illustrated in FIG. 1 (c), a backward-SBS opto-acoustic interaction is particularly designed to take place within a high-Q microtoroid [48] cavity via properly engineering its geometrical size (FIG. 1(a); see supplementary information). In experiment (FIG. 2(a)), a strong pump laser at frequency ω_p is launched to pump the high-energy optical mode (ω_1, k_1), while a weak tunable signal laser at frequency ω_s is, resonant with a resonator mode, employed to excite the low-energy optical mode (ω_2, k_2) instead. Consequently, the counter-propagating signal mode is expected to undergo strong resonant amplification due to the presence of Brillouin phase matching with the strong pump field and an acoustic wave in the same medium. On the contrary, the co-propagating signal laser remains intact owing to the lack of the available Brillouin scattering. It is this unidirectional Brillouin gain that consents to the realization of a functioning optical isolator as well as nonreciprocal PT symmetric dimer.
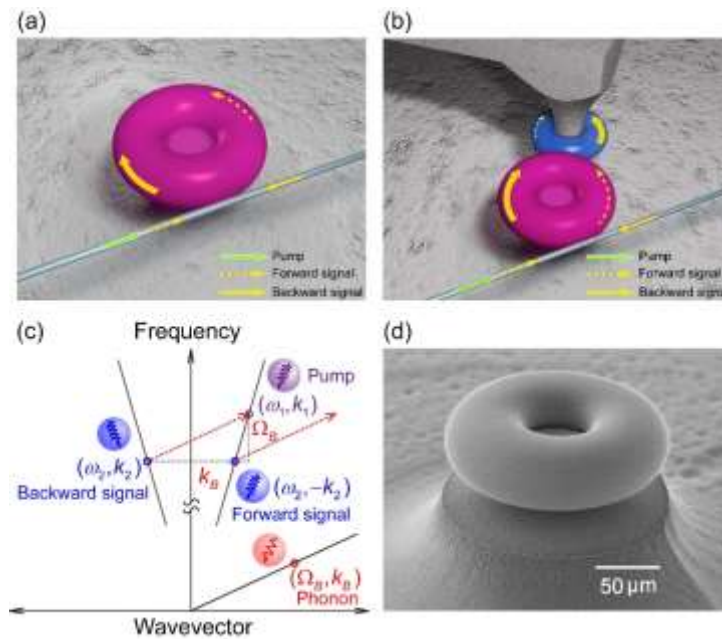

FIG. 1. On-chip optical isolator and nonreciprocal PT symmetry empowered by stimulated Brillouin scattering (SBS) with whispering-gallery-mode silica microtoroid resonators. (a), Schematic illustration of the experiment on optical isolation with a single toroid coupled to a tapered fiber. (b), Schematic of the experiment on nonreciprocal $\mathcal{PT}$-symmetry with two toroids coupled with each other and the active one coupled to a tapered fiber. (c), Schematic illustration of the requirements on phase and energy conservation conditions for the SBS process. (d), SEM image of the Brillouin toroid in our experiments.

As schematically illustrated in FIG. 1(a), our series of isolator experiments are performed simply with a Brillouin microresonator at room temperature and atmospheric pressure by simultaneously launching the signal lights from both forward and backward directions through a tapered fiber coupler for optical interface at 1550 nm. FIG. 1(d) is an SEM image of the fabricated Brillouin microtoroid which has the

principle and minor diameters of 175 μm and 54 μm, respectively. To identify the occurrence of bulk SBS in microtoroid cavity, we first select two high-order optical transverse modes with separation matching the SBS frequency and optically pump the microcavity at the shorter-wavelength mode to above the lasing threshold. As shown in FIG. 2(b), the Brillouin lasing indeed occurs at the longer-wavelength side. The loaded Q factors for the signal and pump waves are measured to be 1.40×10^8 and 4.36×10^7 with respect to their intrinsic Q factors of 1.99×10^8 and 1.04×10^8, respectively.
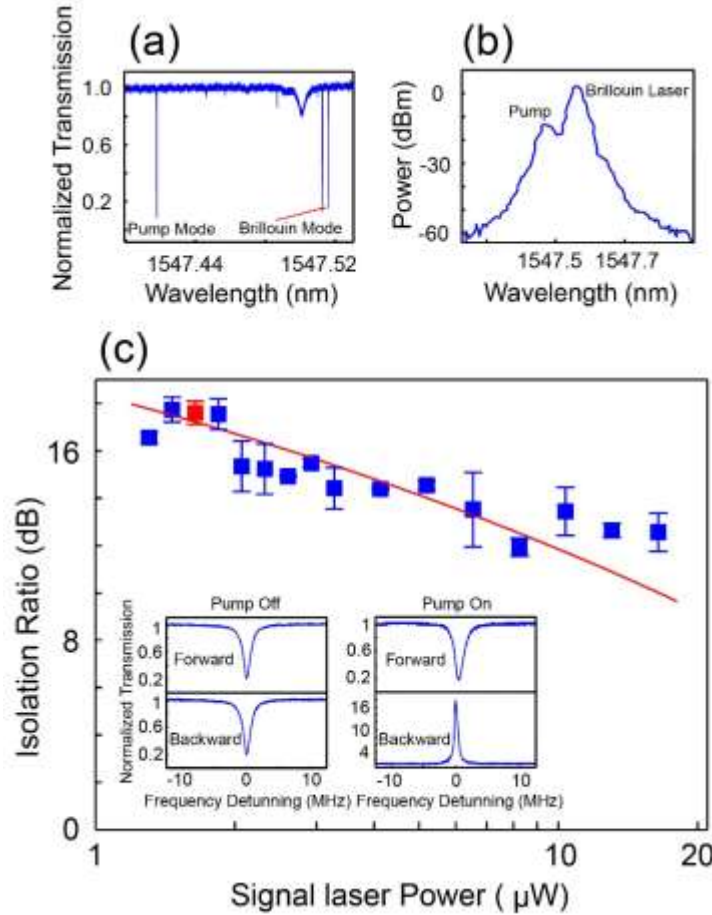

FIG. 2. Optical isolation versus input signal power. (a), Transmission spectrum when scanning the laser wavelength across the microtoroid shown in FIG. 1 (d). (b), Brillouin lasing spectrum. (c), Isolation ratio versus input signal laser power where the equal forward and backward signal laser powers were launched simultaneously from both directions. Inset: Typical transmission spectra corresponding to the red scatter in(c), the red line corresponds to the theoretical curve calculated through the method in supplementary information.

To test the isolation performance of our device, we start with the case of the same input signal powers from both directions but synchronously changing them. In this case, the pump light is thermally locked to the shorter-wavelength cavity mode with a blue frequency detuning. During the measurement, the dropped pump power (determined by the power absorbed within the cavity) keeps at 359.82 μW (below lasing threshold), and the coupling strength κ between the cavity and tapered fiber is also fixed. As a function of the input signal power, the attained isolation ratio is depicted in FIG. 2(c) where the isolation ratio is defined by the peak power of the backward output signal with respect to the dip signal power in the forward direction. From this point of view, the behavior of our isolator bears essential features of a

4

For the launched power range, the isolation ratio is well situated above 11.90 dB and even up to 17.73 dB for the averaged bandwidth of 0.57 MHz. As further indicated in Supplemental Figure. 3, in terms of the injected signal power the achievable isolation bandwidth is mainly limited by the linewidth of the cavity mode as well as the Brillouin gain. The reduction at higher input powers stems from the Brillouin gain saturation (Supplementary information), similar to the reported gain saturation with doped erbium ions [16]. As a comparison, the insets display typical transmission spectra of the output signals as the pump turned on and off for forward and backward configurations. Without the pump, a Lorentzian dip profile is symmetrically observed in both directions in response to the cavity resonance. In contrast, when turning on the pump, the signal transport is dramatically altered: the forward input still remains the same absorption profile whereas the backward input experiences significant amplification.
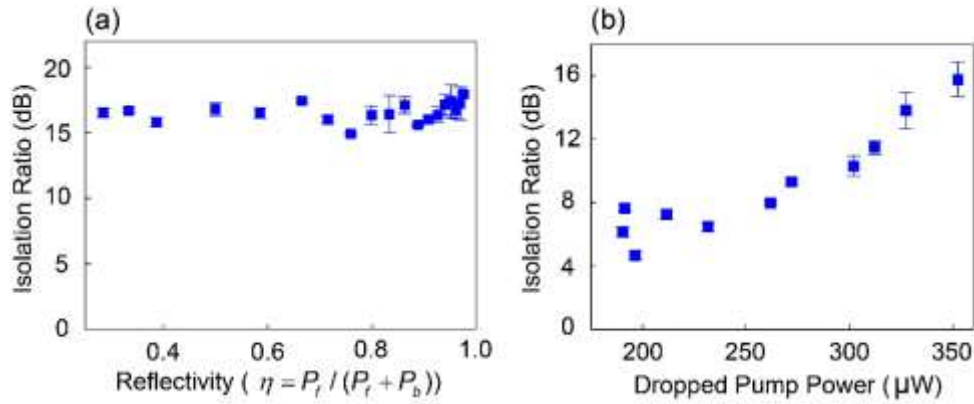

FIG. 3. Isolation performance of the device. (a), Measured optical isolation ratio in terms of the reflectivity $\left(\eta = P_f/(P_f + P_B)\right)$ by setting the backward signal power P_B at 3.28 μW while only varying the power P_f of the forward signal field. The dropped pump power is 359.82 μW and the coupling strength is $2\pi \times 0.39$ MHz. (b), Optical isolation as a function of the dropped pump power by fixing both forward and backward signal powers at 3.28 μW. The coupling strength is $2\pi \times 0.39$ MHz.

Next, we implement the isolation measurements by maintaining the backward input signal power at 3.28 μW while only varying the forward signal power. The dropped pump power and the coupling strength κ are set at 359.82 μW and $2\pi \times 0.39$ MHz. Remarkably, as shown in FIG. 3(a), the isolation ratio stays well above 15 dB for the forward input signal power within the range of 1.31 μW to 130.56 μW. The small fluctuation is mainly due to the instability of the narrow-band tunable optical filter used to filter out the pump light (see Supplemental Figure. 1). To characterize the tunability of our isolator, we further conduct an additional assessment in terms of the dropped pump power. In one set of sampling, the recorded experimental data are plotted in FIG. 3(b) with the same signal input powers from both directions at 3.28 μW and the coupling strength of $2\pi \times 0.39$ MHz. As expected, the isolation ratio starts to grow up along with the increase of the dropped pump power (below lasing threshold). Notice that there is no insertion loss for this device since the signal light is amplified. In comparison with previous results, the SBS-induced optical isolation does reveal a number of advantages ranging from fast switching, great system stability, large system parameter space, to low input signal power.

Thanks to the directional Brillouin gain, the Brillouin microcavity further empowers us to accomplish nonreciprocal PT symmetry by coupling with another passive microtoroid resonator with smaller size. The experimental setup is schematically depicted in FIG. 1(b), where inverted coupling arrangement [55] is adopted. In the experiment, the two microtoroids are mounted on two nanopositioning stages for precise position-separation control. Moreover, we utilize two thermoelectric coolers (TECs) with a temperature stability of 2 mK to individually tune the cavity resonance wavelength via the thermo-optic effect so that both toroids always share the same resonant frequency during the measurements. The loaded Q factors of the Brillouin cavity are measured to be 3.16×10^7 at 1547.5 nm and 2.96×10^7 at 1547.4 nm, respectively, in contrast to their intrinsic Q-factors at 5.41×10^7 and 9.47×10^7. For the lossy microtoroid, its intrinsic Q factor is 9.72×10^7 at 1547.5 nm.

Since the Brillouin gain is only present in the backward configuration, the PT symmetry is investigated under balanced gain and loss for the backward signal input. While for the forward signal, the system is simply two passively coupled microcavities. To avoid the saturation nonlinearity, the dropped pump power is stabilized at 362.32 µW and the input (backward and forward) signal powers are maintained at a low power of 1.10 µW. In addition, the coupling strength κ between the fiber and Brillouin cavity is fixed at $2\pi \times 2.55$ MHz. After carefully balancing the gain and loss in the backward direction, the evolutions of the transmitted signal spectra are presented in FIG. 4(a) by gradually decreasing the coupling strengths $\mu_{f,b}$ between two toroids while maintaining zero cavity frequency detuning. It is apparent that for the backward signal wave, frequency bifurcation induced by PT symmetry exhibits distinct features in spectral location change (FIG. 4(c)) and linewidth narrowing (FIG. 4(b)). In particular, a PT phase transition occurs at the exceptional point where $\mu_b = g = \gamma$. Theoretically, for $\mu_b > \gamma$ the system is in the unbroken phase and two real PT spectral branches $\omega_\pm$ with zero linewidth are quadratically displaced at $\pm\sqrt{\mu_b^2 - \gamma^2}$ away from the central cavity resonance frequency ω_0. When $\mu_b < \gamma$, the PT symmetry spontaneously breaks down and the two spectral eigenvalues $\omega_\pm$ now become a complex conjugate pair. These behaviors have been well confirmed by the experimental results shown in FIG. 4(b) and 4(c). Due to the spectral singularity of the complex optical potential, the significant signal amplification in the backward output (Fig. 4a) also verifies the theoretical prediction by Mostafazadeh [32]. For the forward signal mode, on the contrary, we anticipate to have least outputs at the two supermodes $\varpi_\pm = -i\frac{\gamma + \gamma_g}{2} \pm \sqrt{\mu_f^2 - \left(\frac{\gamma - \gamma_g}{2}\right)^2}$ (see Supplementary information), which are determined by μ_f and the decay rates (γ, γ_g) of the two microresonators. The measured output spectra in FIG. 4 shows excellent agreements with the above theoretical analysis. As such, nonreciprocal PT symmetry is successfully demonstrated in this compound microcavity system. As shown in FIG. 4 (b) and (c), the EPs in two different directions are non-degenerate from each other. A recent theoretical study has shown some intriguing behaviors of this phenomenon [46]. Also, these two EPs show anisotropic behavior, that is, when approached from two different directions, the sensitivity of the deviation of the two supermodes is different. This unique behavior provides us with the possibility to realize a bi-scale supersensitive optical sensor which can detect particles of different sizes at the same time (see supplementary information). A latest study based on two coupled acoustic cavities demonstrated a similar behavior [47].
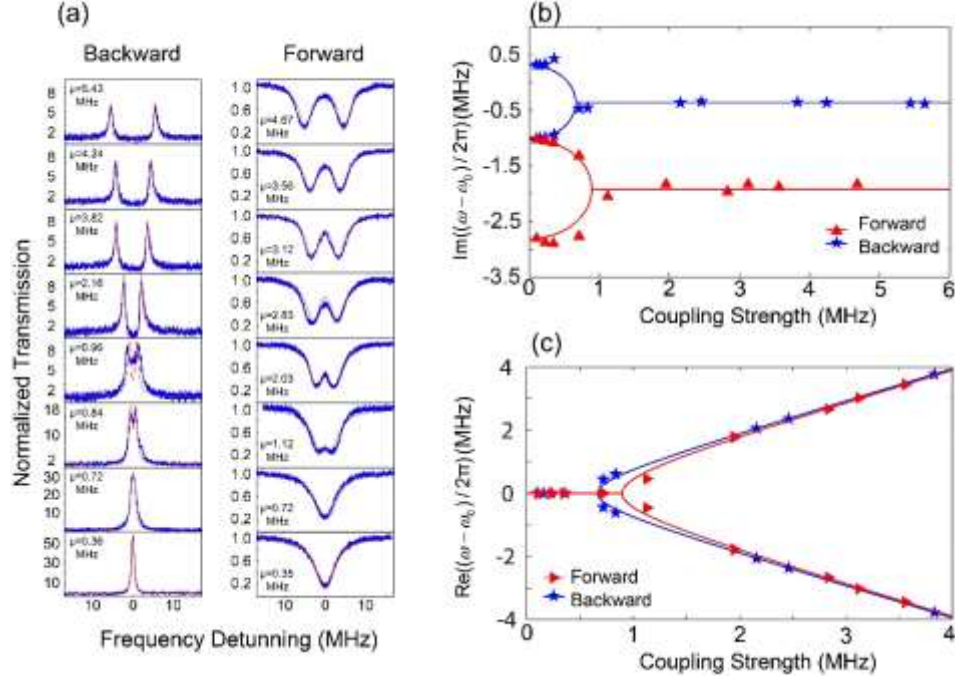
FIG. 4. Transmission spectra in nonreciprocal PT symmetry. (a). Output transmission spectra for forward and backward signal propagation configurations. μ: coupling strength between two cavities. (b) & (c). The imaginary parts and real parts of the two eigenfrequencies of the two supermodes as a function of the coupling strength for forward (red triangle) and backward (blue star) signal propagation configurations. Parameters: the dropped pump power is 362.32 μW and the coupling strength between the active cavity and the fiber is $2\pi \times 2.55$ MHz. (blue: experimental data; red: theoretical curves).

Conclusion.-Unlike previous demonstrations, the bulk SBS-induced optical nonreciprocity offers many appealing features beyond other alternatives. Despite the demonstrated isolation bandwidth is less than 1 MHz, it is believed to be extendable by orders of magnitude with further design optimization including using a microcavity with lower Q-factor or thermally tuning the resonance frequency. From the device integration standpoint, the Brillouin microtoroid resonator has the advantages of compact footprint with CMOS compatibility and reliable isolation functionality, which are crucial in making nonreciprocal elements for on-chip photonic integration. As a fundamental building block, the structure allows a large operating range for the signal power from hundreds of nanowatts to tens of microwatts. Moreover, the scheme could be in principle extendable to squeezed light and continuous variables where phase (in)sensitive parametric amplification is mostly involved in generation. Furthermore, the introduction of nonreciprocal PT symmetry not only affirms the speculation on PT-assisted optical isolation, but also opens up new possibilities for constructing novel PT optical devices outperforming conventional facilities. Although here the SBS is used to demonstrate non-reciprocal PT phase transition, we believe that other direction-sensitive mechanisms can be also exploited to realize the similar phenomenon.

*emails: jxs@nju.edu.cn; mxiao@uark.edu.

[1]. D. Jalas et al., Nat. Photon. **7,** 579 (2013).

[2]. R. J. Potton, Rep. Prog. Phys. **67,** 717 (2004).

[3]. L. Bi et al., Nat. Photon. **5,** 758 (2011).

[4]. B. J. H. Stadler and T. Mizumoto, IEEE Photon. J. **6,** 0600215 (2014).

[5]. Z. Yu and S. Fan, Nat. Photon. **3,** 91 (2009).

[6]. L. D. Tzuang, K. Fang, P. Nussenzveig, S. Fan and M. Lipson, Nat. Photon. **8,** 701 (2014).

[7]. S. Hua et al., Nat. Commun. **7,** 13657 (2016).

[8]. K. Wang et al., Opt. Lett. **42,** 1990 (2017).

[9]. L. Fan et al., Science **335,** 447 (2012).

[10]. M. S. Kang, A. Butsch and P. St. J. Russel, Nat. Photon. **5,** 549 (2011).

[11]. M. Krause, H. Renner and E. Brinkmeyer, Electron. Lett. **44,** 691 (2008).

[12]. X. Huang and S. Fan, J. Lightwave Technol. **29,** 2267 (2011).

[13]. C. G. Poulton et al., Opt. Express **20,** 21235 (2012).

[14]. K. Saha et al., Conference on Lasers and Electro-Optics, paper QF1D.2 (Optical Society of America, 2013).

[15]. L. Chang et al., Nat. Photon. **8,** 524 (2014).

[16]. V. Grigoriev and F. Biancalana, Opt. Lett. **36,** 2131 (2011).

[17]. L. D. Bino et al., Optica **5,** 279 (2018).

[18]. Z. Shen et al., Nat. Photon. **10,** 657 (2016).

[19]. F. Ruesink, M.-A. Miri, A. Alu and E. Verhagen, Nat. Commun. **7,** 13662 (2016).

[20]. K. Fang et al., Nat. Phys. **13,** 465 (2017).

[21]. Z. Shen et al., Nat. commun. **9**, 1797 (2018).

[22]. F. Ruesink et al., Nat. commun. **9**, 1798 (2018).

[23]. J. Kim et al., Nat. Phys. **11,** 275 (2015).

[24]. J. Kim, S. Kim and G. Bahl, Sci. Rep. **7,** 1647 (2017).

[25]. C. Dong et al., Nat. Commun. **6,** 6193 (2015).

[26]. Y. Choi et al., Nat. Commun. **8,** 14154 (2016).

[27]. Y. Shi, Z. Yu and S. Fan, Nat. Photon. **9,** 388 (2015).

[28]. L. Feng, R. El-Ganainy and L. Ge, Nat. Photon. **11,** 752 (2017).

[29]. R. El-Ganainy et al., Nat. Phys. **14,** 11 (2018).

[30]. C. M. Bender and S. Boettcher, Phys. Rev. Lett. **80,** 5243 (1998).

[31]. C. M. Bender, Rep. Prog. Phys. **70,** 947 (2007).

[32]. A. Mostafazadeh, Int. J. Geom. Methods Mod. Phys. **7,** 1191 (2010).

[33]. B. Peng et al., Nat. Phys. **10,** 394 (2014).

[34]. C. E. Ruter et al., Nat. Phys. **6,** 192 (2010).

[35]. L. Feng et al., Nature Mat. **12,** 108 (2013).

[36]. Z. J. Wong et al., Nat. Photon. **10,** 796 (2016).

[37]. L. Feng, Z. J. Wong, R. M. Ma, W. Wang and X. Zhang, Science **346,** 972 (2014).

[38]. H. Hodaei et al., Science **346,** 975 (2014).

[39]. W. Chen et al., Nature **548,** 192 (2017).

[40]. H. Hodaei et al., Nature **548,** 187 (2017).

[41]. A. Regensburger et al., Nature **488,** 167 (2012).

[42]. Z. Zhang et al., Phys. Rev. Lett. **117,** 123601 (2016).

[43]. P. Peng et al., Nat. Phys. **12,** 1139 (2016).

[44]. J. Wen, X. Jiang, L. Jiang and M. Xiao, J. Phys. B: At. Mol. Opt. Phys. **51** 222001 (2018).

[45]. F. Nazari et al., Opt. Express **22,** 9574 (2014).

[46]. A. Y. Song, Y. Shi, Q. Lin and S. Fan, arXiv: 1806.00544v1 (2018).

[47]. K. Ding, G. Ma, Z. Q. Zhang and C. T. Chan, Phys. Rev. Lett. **121,** 085702 (2018).

[48]. D. K. Armani, T. J. Kippenberg, S. M. Spillane and K. J. Vahala, Nature **421,** 925 (2003).

[49]. R. Y. Chiao, C. H. Townes and B. P. Stoicheff, Phys. Rev. Lett. **12,** 592 (1964).

[50]. E. Garmire, New J. Phys. **19,** 011003 (2017).

[51]. H. Lee et al., Nat. Photon. **6,** 369 (2012).

[52]. G. P. Agrawal, *Nonlinear Fiber Optics*, 4th ed. (Chap. 9, Elsevier, Singapore).

[53]. M. Tomes and T. Carmon, Phys. Rev. Lett. **102** 113601 (2009).

[54]. Q. Lu et al., Opt. Lett **41** 1736-1739 (2016).

[55]. G. Li et al., Appl. Phys. Lett. **109,** 261106 (2016).